

Estimation of evaporation and transpiration rates under varying water availability for improving crop management of soybeans using oxygen isotope ratios of pore water**

Gunther C. Liebhard¹ *, Andreas Klik¹ , Christine Stumpp¹ , Angela G. Morales Santos¹ , Josef Eitzinger² ,
and Reinhard Nolz¹ 

¹Department of Water, Atmosphere and Environment, Institute of Soil Physics and Rural Water Management, University of Natural Resources and Life Sciences, Vienna, Muthgasse 18, 1190, Vienna, Austria

²Department of Water, Atmosphere and Environment, Institute of Meteorology and Climatology, University of Natural Resources and Life Sciences, Gregor-Mendel-Straße 33, 1180 Vienna, Austria

Received February 7, 2022; accepted June 8, 2022

Abstract. Knowledge of crop water requirements and the effects of management practices on the amounts of water used for crop transpiration and that lost through soil evaporation is essential for efficient agricultural water management. Therefore, this study investigated the temporal evolution of weekly evaporation and transpiration rates under varying soil water conditions in a conventionally managed soybean field by partitioning evapotranspiration based on a water and $\delta^{18}\text{O}$ -stable isotope mass balance. The estimated rates were considered in combination with vertical soil water distribution, atmospheric demand (based on crop evapotranspiration), actual evapotranspiration, and the plant development stage. This allowed for the weekly rates to be compared to the current conditions resulting from dry periods, rain or irrigation events, and the extent of the canopy. The range of weekly transpiration/evapotranspiration, from blossom to maturation, was between 0.60 (± 0.11) and 0.82 (± 0.10). Within this range, transpiration/evapotranspiration shifted depending on the vertical soil water distribution and meteorological conditions. During dry soil surface periods, evaporation dropped to almost zero, whereas a wet surface layer substantially increased evaporation/evapotranspiration, even under a closed canopy. Under given conditions, the application of a few intense irrigations before the drying of the soil surface is recommended.

Keywords: irrigation, eddy covariance, water scarcity, water use, water stable isotopes

INTRODUCTION

Freshwater is a valuable resource that is experiencing increasing pressure due to a growing demand. One aspect of this growing demand is the expansion and intensification of crop production on irrigated land to stabilize food production (UNESCO, 2020). Currently (and even more so in the future), agricultural production is being challenged by water scarcity (Feres and Soriano, 2006), requiring demand-oriented approaches (Loiskandl and Nolz, 2021; Molden *et al.*, 2003). Sustainable agricultural water management aims at the efficient use of water to preserve water resources and maintain the required yields. Fulfilling the aim of the efficient use of water is attempted by using two approaches. The first approach is to directly increase the water use efficiency (WUE), which is defined as the amount of biomass produced per unit of water used by the crop (Briggs and Shantz, 1913; Nangia, 2020). This approach affects crop performance and thus improves the transpiration efficiency. Differences in transpiration efficiency may be attributed to different carboxylation pathways and energy requirements for the production of diverse plant components (Tanner and Sinclair, 1983). The task of improving WUE may be performed by crop scientists who develop genotypes well adapted to local (dry) environments (Ruggiero *et al.*, 2017), and by plant physiologists and agronomists, who maximize the productivity of the applied water use techniques such

*Corresponding authors e-mail: g.liebhard@boku.ac.at

**This work was supported by the European Union's Horizon 2020 Research and Innovation Programme (Grant number 773903) (2018-2022).

as partial root-zone drying and regulated deficit irrigation (Hedley *et al.*, 2014; Loveys *et al.*, 2004). Regulated deficit irrigation increases WUE by concentrating water application in moisture-sensitive crop growth stages; partial root-zone drying signals the plants to induce a partial reduction in stomatal conductance and shoot growth to reduce water loss by transpiration (Jovanovic and Stikic, 2018). Due to this connection, dry matter partitioning of assimilates from source organs to sink organs (including marketable plant products) and water pressure deficit at leaf surface together with vapor diffusion resistance must be considered (Tanner and Sinclair, 1983). As diffusion resistance may vary between cultivars, Ashley (1983) described the differences between the various soybean cultivars, with photosynthesis being positively correlated to transpiration and negatively to diffusion resistances. The second approach is to increase the fraction of water used for crop transpiration (T) and decrease the fraction of water lost due to soil evaporation (E) by adapting management practices. This affects ET efficiency, which for example, may be pursued by suppressing soil evaporation (Tanner and Sinclair, 1983). Management practices influence the water regime and storage capacity of soils by changing the soil hydraulic properties and soil quality (Sarkar *et al.*, 2020; Strudley *et al.*, 2008). Tillage-associated management, such as mulching, regulates surface wetness and may decrease E. Irrigation management enables the fulfilment of crop water requirements (*i.e.*, transpiration “T”) and reduces unproductive losses (*i.e.*, evaporation “E”). Consequently, the reduction of water loss to the atmosphere through evaporation after the vaporization of liquid soil water from near the soil surface may be achieved by optimizing the time and intensity of irrigation in order to regulate vertical soil water distribution and surface wetness (De Pascale *et al.*, 2011).

In order to improve process understanding and to decrease the fraction of water lost through E, measuring the rate of evapotranspiration (ET) and its fractions, particularly for the crop period and on the relevant on-farm management scales, is necessary. The fundamental correlations on the scale of the ecosystem between E, T, canopy development, and surface moisture are well known from both long-term and large-scale studies. In the case of transpiration under non-water-limiting conditions, they show a close correlation between T with the degree of soil cover and leaf area in plants. Under water-limited conditions, transpiration also shows its sensitivity to changes in water availability and its close correlation to ET. Evaporation, by contrast, correlates closest with near-surface soil wetness (Scott *et al.*, 2020). In order to plan and examine farm management activity, focusing on smaller temporal and spatial scales appears to be a worthwhile endeavour. Investigation of uniform vegetation (crops in particular) under the consideration of actual boundary conditions such as the power of the atmosphere to vaporize and remove water from the vegetated soil surface, vertical soil water distribution, and

the crop growth stage may reveal a more differentiated relationship between E and T under natural (water-limited) conditions as opposed to non-water-limited conditions.

Most commodity crops have been investigated in experimental fields by using various partitioning approaches to improve our understanding of their characteristic water use. The plant-specific ranges of E/ET and T/ET (including the applied partitioning techniques) were reviewed by Kool *et al.* (2014). Investigations into the ecosystem scale naturally comprise areas and periods of water-limited conditions or focus on the impact of limited water availability (Scott *et al.*, 2020); crop-specific field studies often focus on plant-specific E/ET and T/ET under optimum conditions, with soybean as an example (Brisson *et al.*, 1998; Sakuratani, 1987; Sauer *et al.*, 2007; Singer *et al.*, 2010). This focus on well-watered conditions is reasonable because new partitioning approaches are compared and validated with well-tested techniques and models from the literature (*e.g.*, the model by Shuttleworth and Wallace (1985) or the energy and water balance by Lascano *et al.* (1987)) and are thus often based on the characteristic values of a well-developed plant stock. Considering that agricultural production will increasingly occur under conditions of water scarcity, the actual E/ET and T/ET values under varying field conditions are of substantial interest. Therefore, this study aims to investigate the evolution of E and T rates related to varying soil water availability to further provide feedback to farmers regarding the technical guidelines and management activity such as irrigation scheduling.

Two measurement-based approaches comprehensively estimate both fractions of ET. All of the other approaches only estimate either E or T or they are based on analytical or numerical models (Kool *et al.*, 2014). The first measurement-based approach is the carbon dioxide/water vapor correlation-based ET partitioning method using eddy covariance (EC) measurements (Scanlon and Sahu, 2008). It is based on the coherent and simultaneous course of carbon uptake and water loss during T, both of which depend on stomata regulation. The second measurement-based approach used to determine the ratios of the ET fractions is a stable isotope-based partitioning technique using different water isotopologues (Rothfuss *et al.*, 2021; Xiao *et al.*, 2018). Isotope partitioning techniques are based on isotope fractionation processes during phase change. During E, lighter water stable isotopes tend to evaporate more easily than heavy isotopes enriched in the liquid phase (*i.e.*, soil water). This process is more pronounced for oxygen isotopes than for hydrogen isotopes. By contrast, soil water uptake (of glycophytes and mesophytes) does not cause the accumulation of isotopes in soil water (Ehleringer and Dawson, 1992). The differing behaviour of oxygen or hydrogen isotopes during evaporation and transpiration (at root water uptake) allows for the categorization of ET fractions. Both the carbon-water correlation-based approach and the stable isotope-based partitioning techniques have the advantage that they rely for the most part on direct measurements and a few theoretical or

empirical parameters, such as the vegetation-WUE parameter for correlation-based partition (Scanlon and Kustas, 2010) or isotope fractionation factors (Majoube, 1971).

In general terms, the stable isotope analysis of water is an appropriate tool used to investigate both fractions of ET and further aspects of water use efficiency. The studies using various stable water isotope monitoring methods in combination with other measurements to partition ET to E and T on a field or ecosystem scale were reviewed in detail by Rothfuss *et al.* (2021). With a focus on crop water use and intrinsic water use efficiency, stable isotopes have been used to evaluate the effect of water stress, *e.g.* for soybean plants. Welp *et al.* (2008) measured the oxygen isotope ratios of water vapour, leaf water and evapotranspiration water above a soybean canopy in order to investigate the temporal dynamics of $\delta^{18}\text{O}$ ratios in atmospheric waters and ecosystem water pools as well as leaf water enrichment. Bai and Purcell (2018) investigated drought tolerance among soybean genotypes by measuring $^{13}\text{C}/^{12}\text{C}$ ratios in leaves and seeds as a surrogate measurement for water use efficiency and the $^{18}\text{O}/^{16}\text{O}$ ratios in seeds as a surrogate measurement for transpiration. Similarly, Bunce (2019) measured the $^{13}\text{C}/^{12}\text{C}$ ratios in order to determine the differences in water use efficiency for various soybean genotypes at different water vapour deficits. Furthermore, the determination of the $^{18}\text{O}/^{16}\text{O}$ ratios in soybean leaves could be used to investigate the respiratory oxygen uptake and mitochondrial electron transport pathways under water stress conditions (Ribas-Carbo *et al.*, 2005).

As a consequence, a stable isotope-based ET partitioning technique based on $\delta^{18}\text{O}$ measurements in water and soil-water samples was chosen to investigate the E and T rates. Isotope-based techniques have become established in ET research (Rothfuss *et al.*, 2021) but are still less often applied in agricultural investigations than alternative techniques (Kool *et al.*, 2014). Therefore, a water and stable isotope mass balance method from the laboratory was used (Sutanto *et al.*, 2012; Wenninger *et al.*, 2010), which was adapted and tested in field conditions (Liebhard *et al.*, 2022) for the first time, according to our review of the literature, for the analysis of E and T rates under the conditions of varying soil water availability.

The estimated E and T rates derived from the water and stable isotope ($\delta^{18}\text{O}$) mass balance are considered in combination with the actual water status (vertical soil water distribution), atmospheric demand (in the form of crop evapotranspiration, ET_c), actual ET (ET_{act} , from EC measurements), and the plant development stage in order to relate the variation in E and T rates to the current conditions and to explain their temporal evolution. The field investigation as a basis for on-farm management evaluation aims to fulfil the following specific objectives:

i) Determine ET, E/ET and T/ET with respect to the stages in plant development;

ii) Interpret the E/ET and T/ET dynamic with respect to varying water availability;

iii) Draw conclusions with respect to agronomic practices, including irrigation.

MATERIAL AND METHODS

The study was conducted in 2019 in Groß-Enzersdorf (48°12'N, 16°34'E; 157 m elevation a.s.l.), east of Vienna, Austria. The climate may be described as dry-subhumid. In 2009-2018, the annual average precipitation, temperature, and reference ET were 540 mm, 10.6°C, and 840 mm, respectively. The region is characterized by a flat topography and small agricultural fields with intensive farming and irrigation. The experimental field covered an area of 8.5 ha (540 m × 155 m) and had an orientation of 299° to the azimuth (Fig. 1a). The soil type was chernozem with a loamy texture, according to the Austrian nomenclature. The field was conventionally managed based on the decisions of the farmer. The low-growing soybean (*Glycine max* (L.) Merr.) variety (*GL Melanie*) was single-grain seeded (66 plants m⁻²) at the end of a cold, moist spring on April 25, 2019. The field was irrigated using a hose reel irrigation machine on July 23 and August 13 (Days After Seeding [DAS] 89 and 110) to prevent damage to the plants and a substantial reduction in yield caused by the dry, warm summer. On September 3, plots of several square meters were manually harvested for crop yield evaluation. The entire field was mechanically harvested on September 11.

The investigation of the water and $\delta^{18}\text{O}$ -isotope mass balance components focused on the part of the soil-plant-atmosphere system shown in Fig. 2. The upper boundary

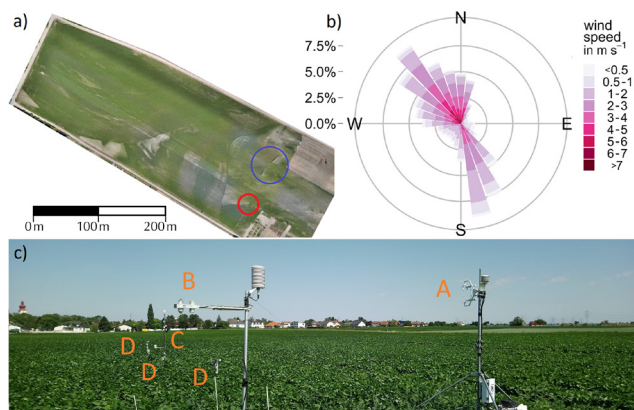


Fig. 1. Experimental field and the arrangement of measurement instruments. a) Aerial (RGB) image of the experimental field on the day after seeding (DAS) 89. The red circle indicates the location of the micrometeorological instrument and the soil water stations. The blue circle indicates the current position of the hose reel irrigation. b) The wind rose based on records from the eddy covariance (EC) anemometer at 2.5 m above ground. c) Image on DAS 69: The beginning of blooming for the soybean stand. A: anemometer and gas analyser, B: Net radiometer, C: Weather station, D: Soil water monitoring stations (water content and matric potential sensors). Rain samplers are not visible in the image.

fluxes comprised precipitation, irrigation, E, and T. The lower boundary fluxes (at the bottom of the effective rooting zone) are comprised of capillary rise and percolation. The storage and transport of water and water vapour within the soil profile were assessed by means of measuring the vertical soil water and stable isotope ($\delta^{18}\text{O}$ and $\delta^2\text{H}$) distribution (Fig. 2). All of the components of the water, stable isotope mass balance, and data contributing to the evaluation (Table 1) were determined in the near vicinity, as close as 15 m, to the micrometeorological instruments and soil water stations. The E and T rates reflect the fluxes at this particular profile and represent the conditions near the measuring station. The weekly evaluation periods covered the plant development stages from the late vegetative growth stage until harvest.

A weather station, including two ADCON Telemetry TR2 air temperature and relative humidity sensors (OTT Hydromet GmbH, Kempten, Germany), was installed near the soil water monitoring sensors in the field (Fig. 1c). An additional rain gauge and a rainwater collector for isotope

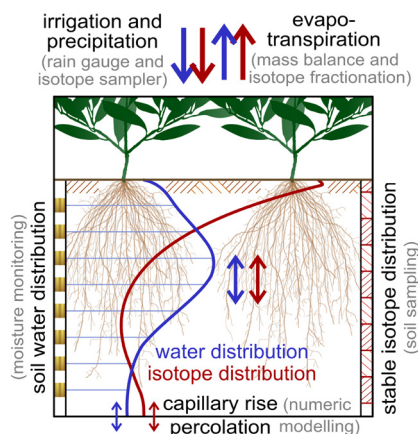


Fig. 2. Water and isotope mass balance components in the soil-vegetation-atmosphere system were measured or calculated to determine the evaporation and transpiration ratios. Characteristic soil moisture and isotope profiles together with applied measurement techniques (in grey font) are shown.

Table 1. Overview of the measured fluxes or parameters and the respective instruments (composite measuring systems) for the determination of the isotope and water mass balance components. Measured fluxes and parameters include evapotranspiration (ET), (Net) radiation (R), soil heat flux (G), sensible heat flux (H), precipitation (Prec.), temperature (T), relative humidity (RH), wind speed (WS), wind direction (WD), and barometric pressure (BP). T and RH were also used for the calculation of isotope fractionation factors

| Category | Water/Isotope | Parameter | Instrument (system) |
|------------|---------------|---------------------------------|--|
| Atmosphere | Water | ET | Water mass balance instruments |
| | | ET (and R, G, H) | Eddy covariance system |
| | | Prec., Irrigation | Rain gauge |
| Soil water | Water | T, RH, Prec., WS, WD, BP | Standard weather station |
| | | Prec., Irrigation | Rain Sampler |
| | | SWC (vert. distr.) | Dielectric impedance reflectometers + Electrical capacitance sensors |
| Soil water | Isotope | Matric potential (vert. distr.) | Electrical resistance type sensors |
| | | Isotope ratios (vert. distr.) | Auger, Isotope and gas concentration analyzer |
| | | Leaf Area Index (LAI) | LAI Ceptometer |
| Crop | | Plant height | Measuring tape |
| | | Root system depth | Measuring tape |
| | | Soil cover fractions | Image analysis tool |
| | | Yield parameters | Crop yield evaluation |

sampling (Rain Sampler RX1, Palmex Ltd, Zagreb, Croatia), which has been proven to suffer from no significant evaporation effect (Gröning *et al.*, 2012), were installed within the field (Fig. 1a). Irrigation samples were taken directly from the tap. The rain gauge used for the water mass balance was installed near the ground between the plant rows to measure the interception losses by the canopy.

The ET for each evaluation period was calculated as the remaining component of a water balance equation. For validation, ET_{act} was additionally measured using an eddy covariance (EC) system.

Three sets of soil probes were installed between the soybean rows near the weather station in the most influential area of the EC flux footprint (Figs 1a and c). The soil water content (SWC) was monitored in the surface layer with Stevens Hydra Probe® soil moisture sensors and using the SDI-12 communication protocol (Stevens Water Monitoring Systems, Inc., Portland, OR, USA) and across the soil profile down to an 80 cm depth using EnviroSCAN® (Sentek Pty Ltd., Stepney, Australia) soil moisture probes. The Hydra Probe readings (temperature-compensated real dielectric permittivity) were related to the volumetric water content ($\text{cm}^3\text{cm}^{-3}$) by applying the appropriate factory calibration (Stevens, 2015), as described by Seyfried, Grant, Du, and Humes (2005). EnviroSCAN readings (scaled frequencies) were converted to the volumetric water content ($\text{cm}^3\text{cm}^{-3}$) by using the standard calibration relationship for sandy loam (Sentek Pty Ltd, 2009). In order to obtain information about soil water retention, each set also contained Watermark® matric potential sensors (Irrometer Co., Riverside, CA, USA) at depths of 20, 40, and 60 cm. These electrical resistance type sensors cover a measuring range from 0 to -200 kPa.

Soil cores for the isotope analysis of pore water were sampled weekly using an auger or core cutter. Samples were collected with an auger in 10 cm depth increments down to 80 cm. Thus, for each pore water isotope sample,

the corresponding volumetric water content was obtained from the in situ measurements. For every depth, three auger samples from between the rows near the soil moisture monitoring station were mixed to create a composite soil sample. This sampling procedure ensured the production of representative and repeatable isotope profiles with deviations of composite samples between 0.02-0.08‰ for $\delta^{18}\text{O}$ (Liebhard *et al.*, 2022). Soil samples from a depth of 0 to 5 cm were taken with a core cutter of 200 cm², which allowed for a thorough excavation of the looser and more granular part of the profile. All soil samples were instantly placed into airtight double zipper plastic freezer bags (double-bagged), which were deflated and stored in a fridge (up to a maximum of 14 days) before analysis.

The mass balance for water and stable isotopes for a considered soil column is:

$$m_{total} = m_i + m_p = m_e + m_f + m_t + m_l, \quad (1)$$

where: m is the mass of water of the different components, labelled according to their subscripts, with the initial (i) and final (f) soil moisture of each sampling period, precipitation plus irrigation (p), evaporation (e), transpiration (t), and percolation (l). Each component may be described as the product of the stable isotope ratio δ ($\delta^{18}\text{O}$) and the fraction of the water in that component x (as $x_j = m_j m_{total}^{-1}$). The components of this isotope mass balance were measured directly ($\delta_i, x_i, \delta_p, x_p, \delta_f, x_f$), and derived from the assumption that the isotope ratio of the transpired water is equal to the isotope ratio of water in the root zone (δ_t), which is calculated from atmospheric conditions and fractionation factors (δ_e), that are considered negligible because of the choice of boundary system (δ_t, x_t), and determined as a residue of the balance calculation (x_t, x_e) in terms of mm d⁻¹. The balance residue x_t could be determined using the following equation:

$$x_t = x_p + x_i - x_e - x_f - x_l, \quad (2)$$

where: the x_t component ($m_j m_{total}^{-1}$) is the balance of the residue from all incoming (precipitation, irrigation) and outgoing (evaporation, percolation) fluxes and the change in storage (initial and final soil water content). To determine x_e , Eq. 1 was formulated as:

$$\sigma_i x_i + \sigma_p x_p = \sigma_e x_e + \sigma_f x_f + \sigma_t x_t + \sigma_l x_l, \quad (3)$$

with each water mass parcel as a product of the factors δ and x . After the substitution of x_t from Eq. (2) δ_e may be expressed as:

$$\sigma_e = \sigma_t - \varepsilon_{total}, \quad (4)$$

with ε_{total} being the sum of equilibrium and kinetic fractionation, Eq. (3) may be converted to:

$$x_e = \frac{x_i \sigma_i + x_p \sigma_p - x_f \sigma_f - x_l \sigma_l - x_t \sigma_t + x_f \sigma_t + x_l \sigma_t - x_l \sigma_l}{-\varepsilon_{total}}. \quad (5)$$

The notations, assumptions, and calculations of the mass balance method were described in detail by Liebhard *et al.* (2022).

The $\delta^{18}\text{O}$ and $\delta^2\text{H}$ isotope ratios of pore water, precipitation, and irrigation samples were analysed using a Picarro L2130-I or L2140-I isotope analyser (Picarro Inc., Sunnyvale, CA, USA). For all measurements, a calibration line was spanned with two laboratory reference standards, which were calibrated twice per year against international standards (USGS 46, USGS 47, USGS 50, and Vienna Standard Mean Ocean Water). The isotope ratios of the liquid samples were calculated from the mean of up to seven measurements for each sample. The isotope ratios of soil water from soil samples were measured based on the H₂O liquid-vapour water equilibration and laser spectroscopy methods (Wassenaar *et al.*, 2008). Therefore, the soil samples or standard water samples in airtight double zipper plastic freezer bags (Ziploc, 17.7x19.5 cm) were inflated with dry air and stored for three days before analysis in order to reach an equilibrium in the headspace of the bag. The samples were manually analysed by means of puncturing the bags with a needle and establishing a continual air flow to the Picarro analyser chamber. For data normalization and instrumental drift correction, the standard was measured before and after three soil samples were taken. The characteristic sample values were determined from 1-minute mean values after a constant measured value was reached for at least 2 min. All of the measured ratios were normalized to the internal standards and expressed in terms of delta notation δ with reference to the Vienna Standard Mean Ocean Water (Craig, 1961). The impact of isotope fractionation was graphically identified by comparing the water samples to the local meteoric water line (LMWL, $\delta^2\text{H} = 6.67 \delta^{18}\text{O} - 1.77$), which in turn was based on precipitation data from Vienna (IAEA, 2020) (IAEA database WISER; accessed on December 22, 2020). Details of soil water sampling and isotope analysis are described in Liebhard *et al.* (2022).

Uncertainties in the calculations of E and T rates were estimated by using the Taylor Series Method (TSM) for uncertainty propagation. The uncertainty propagation estimation considered the uncertainties associated with sampling, measurements, and the underlying assumptions for the water and stable isotope mass balance components and was supported by use of the R package “propagate”. With regard to isotope balance components, the isotope ratios of the precipitation and irrigation samples were derived from seven measurements with standard deviations ranging from 0.01 to 0.05‰ (for $\delta^{18}\text{O}$). Sampling errors that were due to enrichment in the rain sampler within the weekly sampling periods were not considered, as the isotopic enrichment after 30 days in the sampler used was reported to have 0.02‰ ($\delta^{18}\text{O}$) (Gröning *et al.*, 2012). The isotope ratios of the composite soil water samples, which were mixed from each of the three subsamples close to the water monitoring station, had standard deviations ranging from 0.03 to 0.12‰ for $\delta^{18}\text{O}$. However, the standard deviation for the error propagation was based on an averaged

long-term error of 0.18‰ for $\delta^{18}\text{O}$ (Liebhard *et al.*, 2022). The assumption of the isotope ratio of transpired water being equal to the isotope ratio of soil water in the root zone was assumed to be appropriate. The related uncertainties were not quantified and considered, as fractionation at the point of root water uptake of soybean is negligible (Ellsworth and Williams, 2007). With regard to water mass balance, all of the measurements were directly performed at the monitoring station, thereby representing the local conditions and not considering the spatial variability of the local soil, hydrology or plant cover. Nevertheless, determining the water mass balance components was related to the highest degree of uncertainty. Differences in the cumulative amount of precipitation for each evaluation period between the weather station at the water monitoring station and a nearby (approx. 120 m) weather station by the Central Institute for Meteorology and Geodynamics, Austria (ZAMG), were between 0.75 and 3.20% (considering only periods with summed precipitation amount >10 mm). Considering the uncertainties of soil water monitoring, the calibration of the EnviroSCAN capacitance sensors in the laboratory before installation in the field probably caused overestimation near saturation and underestimation during dry conditions (Evet *et al.*, 2012, 2009). Based on experiments with similar soil (Paltineanu and Starr, 1997), the measuring uncertainties were considered with a standard deviation of $0.031 \text{ cm}^3\text{cm}^{-3}$. With regard to the uncertainties associated with quantifying isotope enrichment due to fractionation processes, the uncertainties were considered through measuring inaccuracies given by the sensor manufacturers without quantifying the level of uncertainty of theoretical fractionation relationships. For the temperature-dependent calculation of equilibrium fractionation factors, the experiments of Horita and Wesolowski (1994) supported the accuracy of and the relationship between the applied temperature-dependent equations that were determined by Majoube (1971). Similarly, the high degree of accuracy of the applied humidity-dependent calculation of kinetic fractionation factors by Gonfiantini (1986) was validated theoretically and experimentally (Clark and Fritz, 2013).

A profile depth of 80 cm accounts for the direct impact of evaporation and soybean root water uptake on the soil water as well as the isotope distribution for the local soil and meteorological conditions (Liebhard *et al.*, 2022). With the lower system boundary set to an 80 cm depth, an assumption was made that the water and isotope fluxes at the lower system boundary were negligible. With regard to outflow, percolation was considered to be negligible below the rooting zone, because ET typically exceeds precipitation in areas with chernozem soil, because this is a characteristic of pedogenesis (Eyre, 2017). With regard to inflow, the influence of capillary rise from below an 80 cm depth (gravel layer) was also excluded (mean groundwater level greater 5 m below surface). A Hydrus-1D numerical simulation (Šimůnek *et al.*, 1998) was performed to verify

this assumption. The model was set up in seven layers using the single-porosity van Genuchten-Mualem model without hysteresis, with observed atmospheric boundary conditions, and free drainage at the lower boundary (gravel layer). Daily ET_c was calculated based on the FAO dual crop coefficient approach. The soil surface resistance of the bare soil was determined according to the method of Stroosnijder (1987). The minimum allowed pressure head (h_{CritA}) at the soil surface as the limit for potential evaporation was restricted to a height of -250 m . The height restriction for h_{CritA} was initially calculated from weather conditions and subsequently adjusted to the retention curve of the surface layer. The root water uptake of soybean was calculated using the built-in Feddes model. The leaf area index (LAI) was considered to have a radiation extinction constant of 0.463, as specified in the manual (Šimůnek *et al.*, 2012). Rain interception was considered to be that proposed by von Hoyningen-Huene (1983). The observed root system depths and LAIs are provided in tabular form as input data. The calibration of the hydraulic parameters was performed by minimizing the objective function with the built-in Marquardt-Levenberg parameter estimation technique based on the observed SWC data from before the balance calculation period. Observation nodes for calibration and simulation were defined which corresponded to the selected SWC sensor depths (10, 20, 40, 60, and 80 cm). The initial soil profile conditions were set to the actual SWC values.

Plant development was monitored weekly. The recordings comprised plant height, phenological stages, root system depths, LAI, and soil cover fractions. Plant heights and root system depths were measured with measuring tapes. For the root system depths, trenches were excavated to measure the maximum root depth of the tap root. The phenological development stages were determined according to Meier (2018) and given as BBCH stages. LAI was measured using an AccuPAR PAR/LAI Ceptometer Model LP-80 (METER Group, Inc. USA), and soil cover fractions were determined using an image analysis tool (Bauer and Strauss, 2014). The soil cover fractions comprised the fractions of canopy cover (living plants), residues (dead plant material), and bare soil in percentage terms.

Daily actual and potential ET results were additionally determined to validate ET from the water mass balance and to assess the E and T rates based on the water mass balance in relation to atmospheric conditions and water availability.

Actual ET – which is almost linearly proportional to the latent heat flux – was estimated using an eddy covariance (EC) technique, which has proved to be adequate for assessing ET on a field scale (Foken *et al.*, 2012). Thus, turbulent fluxes were derived based on an EC system that measured latent (LE), sensible (H), and soil heat flux (G), as well as net radiation (R). Its core devices were a high-frequency open-path $\text{CO}_2/\text{H}_2\text{O}$ gas analyser (EC150) and a 3D sonic

anemometer (CSAT3A) combined with an EC100 electronic module (all Campbell Scientific, Inc., Logan, USA). Additionally, a net radiometer (CNR1, Kipp & Zonen B.V., Delft, Netherlands), soil heat flux plates (HFP01, Hukseflux Thermal Sensors B.V., Delft, Netherlands), soil thermocouple probes (TCAV), water content reflectometers (CS615), and temperature and relative humidity probes (HMP35C, all three Campbell Scientific, Inc., Logan, USA) were installed with radiation shields. The micrometeorological devices were installed on May 2, 2019, (DAS 7) in a position within the field that took account of the prevailing wind directions from the northwest (Fig. 1b). Thus, the EC measurements aimed to reflect the magnitude and temporal dynamics of ET in the entire field as a comparative reference point and validation of ET rates at the measurement station. The anemometer and gas analyser were mounted 2.5 m above ground level. With this installation height, the flux footprint was weighted near the measurement stations and covered the extent of the field. The net radiometer was installed at a height of 2.2 m facing due south. In order to determine the soil heat flux, two sets of sensors were installed horizontally in the undisturbed soil. Two soil heat flux plates were installed in a horizontal position approximately 8 cm below the surface. The SWC sensors (CS615 WC reflectometers) comprise two 30 cm long parallel rods with a 3.2 cm spacing that served as waveguides for SWC measurements based on time domain principles. The rods were installed in a horizontal position at different depths: the first reflectometer with the upper rod resting approximately 2.5 cm below the surface and the lower rod at 5.7 cm, and the second reflectometer with the upper rod resting approximately 8.0 cm below the surface and the lower rod at 11.2 cm. The thermocouple sensors were installed approximately 2 and 6 cm below the surface. With these settings, the soil heat flux at the soil surface was calculated as the sum of the measured heat flux at 8 cm and the storage term. Therefore, the dry bulk density and specific heat capacity of the soil are required. The dry bulk density determined from the core samples was 1.41 g cm^{-3} . A heat capacity of $840 \text{ J kg}^{-1} \text{ K}^{-1}$ was derived from chernozem soils with similar properties (Kodešová *et al.*, 2013). The sampling frequency was 20 Hz. Raw data were stored on a CR3000 micrologger and processed using EasyFlux DL software (both Campbell Scientific, Inc., Logan, USA) to obtain 15 minute values. The pre-processing of the high-frequency time series comprised despiking and filtering, frequency corrections using cospectra (Moore, 1986), sonic sensible heat flux correction (Schotanus *et al.*, 1983), line/volume averaging (Foken *et al.*, 2012b), sensor separation (Foken *et al.*, 2012b), correction for air density fluctuations (Webb *et al.*, 1980), data quality classification (Foken *et al.*, 2012b), and density correction “WPL” as recommended by the manufacturer (Campbell Scientific, Inc., Logan, USA). Values were excluded when the wind was from directions where the distance to the field border was below

120 m to only ensure the consideration of ET from within the field. The energy balance closure for the described data filter was 0.80 ($R^2=0.97$). This balance closure for a field investigation was regarded as acceptable, considering that a typical mean imbalance is of the order of 20% in EC measurements (available energy is larger than the sum of the turbulent vertical heat fluxes) due to deviations from the theoretical requirements, measurement inaccuracies, incorrect sensor configurations, and scale problems (Foken, 2008; Masseroni *et al.*, 2014). Residues from the energy balance were allocated to the LE component, considering the Bowen ratios according to Pan *et al.* (2017).

The potential ET was determined in terms of crop evapotranspiration (ET_c) using the FAO dual crop coefficient approach (Allen *et al.*, 1998). Accordingly, ET_c was calculated as the product of the reference ET (ET_0) and the summed crop coefficients ($K_{cb}+K_e$). ET_0 was calculated using the ASCE standardized reference ET equation (Allen *et al.*, 2005). The required input data were obtained from the weather station and the EC measuring system. The crop coefficients were adapted using meteorological, soil property, and crop development data. The basal crop coefficient K_{cb} (defined as ET_c/ET_0) represents T at a potential rate and residual E from the dry surface beneath the dense vegetation. The tabulated K_{cb} coefficients for the initial, mid, and end growth stage from the guidelines were corrected by using the measured daily wind speed, minimum relative humidity, and plant height data according to Allen *et al.* (1998), which resulted in K_{cb} values of 0.14, 1.05, and 0.23. $K_{cb}+K_e$ also included E from the wet topsoil and accounted for the effects of specific wetting events. In the calculation, E was restricted by the available energy at the soil surface and the grade of exposure. For every drying process after a wetting event, E was reduced by an E reduction coefficient (K_r), depending on the soil properties (total evaporable water of 31.3 mm, readily evaporable water of 12.1 mm), the already evaporated water and a coefficient taking the canopy into account, and also representing the soil fraction that was both wet and exposed to incoming radiation (Allen *et al.*, 1998).

RESULTS AND DISCUSSION

In the dual-isotope plot (Fig. 3), which presents alterations in the $\delta^2\text{H} - \delta^{18}\text{O}$ relationship in soil water samples due to evaporation fractionation, results from the pore water samples either plot close to the LMWL or below it. In particular, the samples from the top 20 cm of the soil profile indicate isotope enrichment due to fractionation processes during E.

The isotope ratios of soil water samples from 0 to 60 cm were distributed along a linear regression line ($R^2=0.91$, black line), with a slope smaller than the LMWL (blue line). The positions of the soil water sample isotope ratios apart from the LMWL indicate that

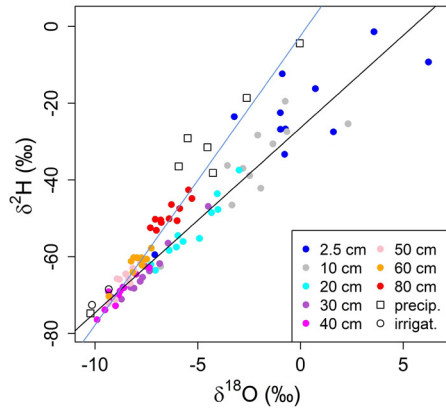


Fig. 3. Dual-isotope plot of weekly soil water, precipitation, and irrigation samples plotted against the Vienna Standard Mean Ocean Water. Local Meteoric Water Line (LMWL, in blue) based on the precipitation data from nearby Vienna (IAEA database WISER). Soil water isotope trend line (in black) as a regression line from soil water samples down to a 50 cm depth.

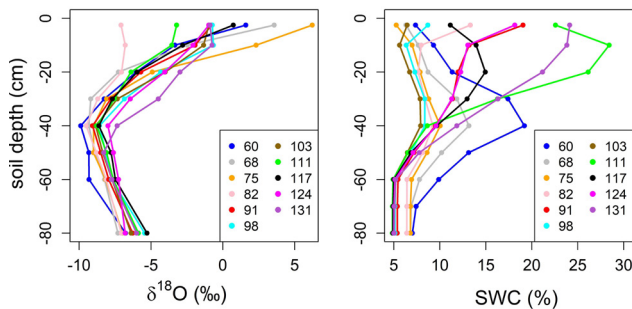


Fig. 4. Isotope and soil water content (SWC) profiles. Profiles for sampling dates (days after seeding). The isotope ratios were derived from composite samples, SWC was averaged from three soil moisture stations.

the soil water samples experienced equilibrium fractionation. This indicates the removal of evaporated soil water by the wind and thus kinetic fractionation processes. Two samples (marked with arrows) from the surface layer (blue circles) and samples from below a 60 cm depth were near the original source water ratio (LMWL); hence, they were

similar to the meteoric samples and may be regarded as being less affected by non-equilibrium fractionation processes. The isotope ratio of the surface soil water samples (2.5 cm depth) near the LMWL ($-3.2 \delta^{18}\text{O}/-23.5 \delta^2\text{H}$ and $-0.9 \delta^{18}\text{O}/-12.4 \delta^2\text{H}$) originated from sampling immediately after irrigation events (DAS 111, 131, Fig. 4, and Fig. 5e); thus, they were not affected much by E. This information derived from isotope depth sampling suggests that the soil water at these depths already shows seasonal variation and originated from previous periods with low evaporative demand and considerable rainfall that percolated into deeper layers. Consequently, the monitoring and sampling depth of this study included the relevant soil profile being influenced by evaporation during the vegetation period. Low moisture gradients were found at the lower system boundaries during the vegetation period (Fig. 4).

The isotope soil water profiles from the vegetation period showed a steady profile with little variability over time compared with the variation in isotope profiles in environments with comparable meteorological conditions and plant cover (Dubbert and Werner, 2019). This may be attributed to isotope equilibrium conditions below the soil surface during the evaluation period, with dry conditions and little downward movement of precipitation or irrigation waters and the redistribution of water and water stable isotopes. Furthermore, the final root system depth was almost reached at the beginning of the evaluation period. Only profiles from measurement dates following a larger precipitation or irrigation event (DAS 82, 111) or a longer dry period (DAS 75) deviated from the characteristic shape (Fig. 4, Fig. 5e), particularly in the top 20 cm soil depth. Even after the first irrigation (DAS 91) and lesser rain events, the high atmospheric capability to vaporize and remove water from the moist surface (Figs 5c, d, and f) caused increased isotopic enrichment in the shallow soil layers and prompted convergence to the characteristic summer profile, this was also described by Allison (1998) for arid regions. The last two profiles (DAS 124, 131) already

Table 2. Transpiration (T), evaporation (E), and crop parameters for each weekly sample period. T and E were estimated based on the water and stable isotope mass balance, ET_c from the FAO dual crop coefficient approach, and ET_{act} from the water mass balance. Plant development (BBCH) macroscales (selection): 20-40: vegetative development, 50: formation of blossoms, 60: blossom, 70: fruit and seed development, 80: fruit and seed maturation, 90: dieback. Leaf Area Indices overlapped due to spatial inhomogeneities

| Period | I | II | III | IV | V | VI | VII | VIII | IX | X |
|---|------------|------------|------------|------------|------------|------------|------------|------------|------------|-------------|
| Period (DAS) | 60-67 | 68-74 | 75-81 | 82-90 | 91-97 | 98-102 | 103-110 | 111-116 | 117-123 | 124-130 |
| BBCH stages | 27-51 | 51-61 | 61-65 | 64-69 | 69-74 | 72-77 | 74-83 | 78-93 | 92-97 | 96-99 |
| Canopy cover (%) | 78-95 | 95-98 | 98-99 | 99-99 | 99-99 | 99-98 | 98-53 | 53-15 | 15-06 | 06-03 |
| Cum. irrig. + precip. (mm) | 2.2 | 2.6 | 19.9 | 43.8 | 3.0 | 3.2 | 72.9 | 1.0 | 17.5 | 41.4 |
| Rel. hum. (%) | 60.1 | 56.7 | 66.5 | 63.7 | 73.7 | 65.0 | 71.3 | 63.8 | 75.3 | 76.8 |
| Averaged air temp. (°C) | 24.9 | 22.2 | 18.3 | 22.8 | 23.7 | 21.6 | 23.4 | 21.5 | 21.8 | 21.9 |
| Aaver. daily glob. rad. (MJ m ⁻²) | 327 | 278 | 225 | 277 | 227 | 232 | 225 | 234 | 171 | 183 |
| Leaf area index | 1.3-2.1 | 2.1-3.8 | 3.8-4.0 | 4.0-3.7 | 3.7-2.9 | 2.9-2.7 | 2.7-2.0 | 2.0-1.5 | 1.5-1.3 | 1.3-1.1 |
| ET_c (mm d ⁻¹) | 6.1 | 5.8 | 4.5 | 5.5 | 5.0 | 4.7 | 4.8 | 4.3 | 2.4 | 3.4 |
| ET_{act} (mm d ⁻¹) | 5.9 | 4.5 | 3.6 | 3.6 | 3.8 | 2.5 | 3.0 | 3.4 | 2.0 | 1.7 |
| T (mm d ⁻¹) | 4.2 (±0.3) | 2.8 (±0.3) | 2.1 (±0.4) | 2.3 (±0.2) | 2.8 (±0.2) | 2.0 (±0.3) | 2.3 (±0.3) | 2.7 (±0.3) | 1.1 (±0.2) | -0.1 (±0.3) |
| E (mm d ⁻¹) | 1.7 (±0.2) | 1.7 (±0.2) | 1.5 (±0.3) | 1.3 (±0.1) | 1.1 (±0.2) | 0.5 (±0.2) | 0.7 (±0.2) | 0.7 (±0.1) | 1.0 (±0.1) | 1.7 (±0.2) |
| $T_{/ET} / E_{/ET}$ | 0.71/0.29 | 0.62/0.38 | 0.60/0.40 | 0.65/0.35 | 0.72/0.28 | 0.82/0.18 | 0.78/0.22 | 0.80/0.20 | 0.52/0.48 | -0.03/1.03 |
| | (±0.06) | (±0.06) | (±0.11) | (±0.06) | (±0.06) | (±0.10) | (±0.11) | (±0.08) | (±0.12) | (±0.18) |

reflected the beginning of the curve shift downward during the period with reduced vegetation and an increased infiltration of rainfall water that was less affected by evaporation and thus the fractionation processes.

Table 2 shows the T and E fractions with the corresponding development stages and plant development parameters for the weekly evaluation periods from inflorescence emergence to maturity and harvest. As the sampling intervals

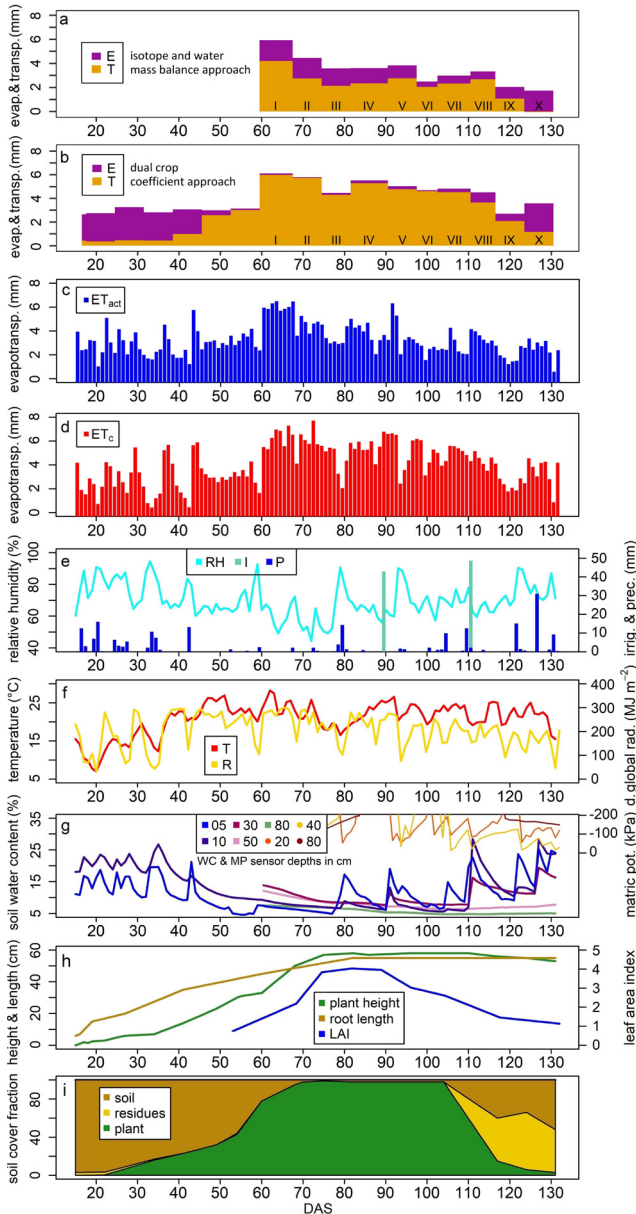


Fig. 5. a) Evaporation (E) and transpiration (T) fractions for evaluation periods from the mass balance approach, b) E and T from the dual crop coefficient approach, c) daily values of actual ET (from Eddy Covariance), d) daily values of potential ET (from the dual crop coefficient approach) and parameters describing e+, f) weather, g) soil moisture, h) plant development, and i) soil cover. Dates in days after seeding (DAS). Continuous soil water content recordings below 10 cm only from DAS 60. Matric potential measurements only from DAS 75 and in a measuring range from 0 to -200 kPa.

varied but were always approximately one week, E and T were converted to rates, expressed as millimetres per day, representing average values within the respective period.

The T fractions of the periods before maturity ranged between 60 and 82%. This range is in line with the range revealed by other studies on soybean (Sakuratani, 1987; Sauer *et al.*, 2007; Singer *et al.*, 2010). However, the temporal evolution of the T fraction during the evaluation period did not strictly progress according to the crop parameters. The highest T/ET ratios were calculated for Periods I, V, VI, and VIII, although plant development had as yet not been completed in Period I, and maturity had already begun in Period VIII. The temporal variability of the T and E fractions may be explained by considering certain influencing parameters such as the daily global radiation, vertical SW distribution, and canopy development (Figs 5f-h).

Beginning with DAS 35, increasing solar radiation and vegetative growth led to a decrease in soil moisture (soil moisture monitoring below 10 cm worked continuously only after DAS 60). Nonetheless, the soil water storage was still sufficient to enable an actual ET to occur (ET_{act} , Fig. 5c) that was close to the potential ET (as ET_c , Fig. 5d) until approximately DAS 70, including the first evaluation period (DAS 60-67). Therefore, the E (29%) and T (71%) fractions represented the ratio of soybean plants that were still in the development stage, with no water stress and almost complete canopy cover. E was approximately 1.7 mm d^{-1} , this was similar to the later periods, and T reached its maximum at approximately 4.2 mm d^{-1} . With the depletion of soil water and a decreasing level of available energy (Figs 5f and g), ET decreased, although the canopy was still developing, and the plants reached their full extent later on at approximately DAS 75 (Fig. 5a). During phases I-III the decrease in T was greater (from 4.2 to approximately 2.1 mm d^{-1}) than the decrease in E (from 1.7 to 1.5 mm d^{-1}). The rain events that occurred on approximately DAS 79 (cumulated 20 mm) only wetted the canopy and surface layer and evaporated for the most part. Irrigation on DAS 89 (43 mm) also contributed to E during periods IV and V, but this water could have been used by the plants and increased T/ET. One third of the irrigation water already evaporated or transpired within three days (DAS 90-92) of high atmospheric demand, and the topsoil rapidly dried out (Figs 5c, d, and g). As the plants were already suffering from drought stress, with effects as identifiable on ET_{act} in comparison with ET_c (Figs 5a-d) and crop yield parameters (Table 3), T/ET increased in Period V. This development continued during Period VI. Therefore, E dropped below 0.5 mm d^{-1} , and T was 2.0 mm d^{-1} . As the topsoil dried out, the stressed plants continued to take water from the root zone throughout the evaluation period. The T rate remained constant, although the balance between water availability and evaporative demand varied, which caused a varying matric potential difference (Fig. 5g). This compensation may be attributed to stomatal regulation, which increases

WUE in response to a slight soil water deficit (slight soil water deficit as a parameter of pot-plant experiments with a fraction of transpirable soil water [FTSW] >0.30) (Liu *et al.*, 2005). After minor rain events on approximately DAS 104 (cum. 15 mm), T and E increased to 2.3 mm d⁻¹ and 0.7 mm d⁻¹, respectively (VII). The second irrigation on DAS 110 caused an increase in ET to 4.1 mm d⁻¹, which steadily declined to 1.4 mm d⁻¹ until DAS 119 (Fig. 5c). The initial wetting from the rain event resulted in an improved infiltration to deeper soil layers than from the first irrigation, which was applied after ten days without rain. Therefore, Period VIII from DAS 111-117 showed a remarkably high T/E ratio, which could be attributed to the available soil water in the root zone and an LAI value which remained high in combination with the first fallen leaves creating a protective mulch layer (Figs 5g-i). As maturation proceeded rapidly, the T/ET value decreased to zero, which was expected and confirmed that the method provided plausible results.

The first evaluation period covered the late vegetative development stage just before the full canopy state was reached at approximately Period III. Until that period, soil water was sufficient to fulfil plant requirements, which promoted both E and T and maintained ET_{act} at a similar level to ET_c. Therefore, periods I and II had the highest ET rates throughout the vegetation period. From Period IV onward, ET was mainly restricted by a limited soil water availability. As a consequence, there was no more direct dependency between the fraction of T and the canopy cover (*i.e.*, LAI) as described by Wu *et al.* (2017) and for a large scale as described by Scott *et al.* (2020). The temporal evolution of E/ET and T/ET agrees with the results reported by Sakuratani (1987), where E from an early stage soybean plant with a sparse canopy was already similar to ET from a fully developed field with a dense canopy and decreased with increasing LAI. The E rate decreased until the full canopy was reached and only significantly increased at the beginning of maturation. Individual periods of lower rates were

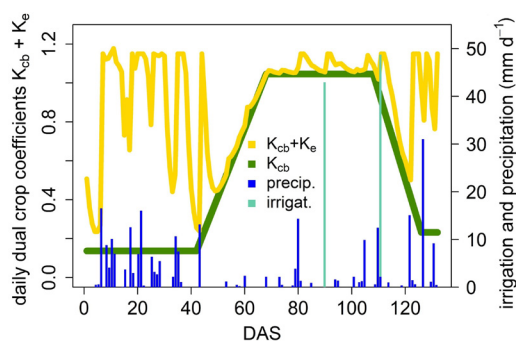


Fig. 6. The daily progression of the FAO dual crop coefficients for the calculation of potential evapotranspiration. Dates in days after seeding (DAS). The crop coefficient Kcb represents potential transpiration plus evaporation from the dry soil surface. Ke represents additional evaporation from the wet topsoil caused by specific wetting events.

attributed to the dryness of the surface layer. Furthermore, high E rates during the first evaluation periods representing the vegetative development stage (periods I-II; DAS 60-75) contributed to the higher ET rates as compared to those during full plant development with several canopy layers (periods III-V; DAS 75-97). This high rate of unproductive water loss through E during the early growing season with multiple rain events (DAS 15-42) was also indicated by the results of a potential E and T rate calculation using the dual crop coefficient approach (Fig. 5b, Fig. 6).

The water stress conditions (ET_{act}=389 mm and ET_c=472 mm for DAS 15-131) caused differing E and T ratios as compared to the ratios under well-watered conditions from the dual crop coefficient approach (Figs 5a and b). The potential ET data based on the dual crop coefficient approach from this growing season indicated a similar water loss potential for the initial evaluation period (DAS 60-67), the bare soil was exposed to a high evaporation demand similar to the periods with a full canopy (*e.g.* periods IV & V, DAS 82-97). This high water loss potential in the initial evaluation period (DAS 60-67) suggests that an earlier sowing date or effective soil cover could have decreased unproductive water loss. However, although the full canopy provided effective cover, E rates remained at approximately 1.45 mm d⁻¹ for periods with an increased surface wetness from immediate rain events (Table 2, Fig. 5g). These measured E rates showed that the dual crop coefficient approach overestimated the protective function of a full canopy. The substantial E rates that occur, even under a full canopy supports the assumption that the LAI effect on T/ET was limited and became insensitive to further increases in LAI (Brisson *et al.*, 1998). According to the definition of this limiting threshold by Ritchie and Burnett (1971), where T/ET_c reached 90%, Sakuratani (1987) estimated an LAI of 2.6 for soybean, which agreed with the ratios determined in this study (Fig. 5a, Table 2). The proportion of E was not only high due to limited T but also because of several minor rain events intercepted by the canopy that only wetted the top few centimetres of the soil (Fig. 5g). In general, the calculated ratios also agreed with the results of Brisson *et al.* (1998), who showed significant E rates and high daily dynamics, even for closed soybean canopies. Furthermore they showed that daily E could account for two-thirds of ET for the moist topsoil (*e.g.*, with frequent irrigation). Taking into account the high E value in the case of moist surfaces even for closed canopies, the two irrigation events shortly before periods V and VIII were used efficiently for T. The irrigation water contributed to E mainly in the first days after their application and percolated to the deeper root zone. The SWC in the surface layer rapidly decreased to moderate soil moisture, still lowering vapour pressure deficit conditions below the canopy and consequently reducing evaporative demand. By contrast, the steady atmospheric demand (*e.g.*, temperature and global radiation; Fig. 5f) maintained the effect of transpiration

pull and caused high T. At the beginning of maturation, the canopy lost its protective cover. The evaporated and transpired water vapour was removed by turbulence as the canopy thinned out. It is noteworthy that the soil surface was protected from the first fallen leaves, which shielded it from incoming radiation, reduced the removal of water vapour, and thus may have been responsible for limiting actual evaporation (Figs 5c, d, and g).

Based on weekly time steps, distinguishing the effects of individual factors, such as the effect of irrigation events, was difficult. However, weekly intervals are reasonable for investigating the E and T ratio-dynamics for the entire vegetation cycle or comparing management strategies. For improved determination and the quantification of individual influencing factors, shorter intervals and additional sampling immediately before and after irrigation would be beneficial. For the selected periods, shorter sampling intervals would more clearly distinguish correlations, such as a comparison of daily values of irrigation (Fig. 5e) and summed ETs (Fig. 5c). Overly long sampling intervals only show a combination of the effects of several factors (*e.g.*, radiation, canopy, water availability) and causal long-term correlations such as that of the canopy with T. Furthermore, for the comprehensive consideration of plant water use, effects on T efficiency should be considered, although certain related parameters (*e.g.*, leaf water status, gas exchange parameters) were not measured in this study. E as a part of ET should not be directly associated with water loss because it decreases the vapour pressure deficit at the plant level, particularly when there is a very dense canopy and low atmospheric turbulence (Gordon, 1940; Kucera, 1954). This decrease not only reduces transpiration pull and water stress but also improves WUE by enhancing plant water productivity (Jiao *et al.*, 2019; Rawson *et al.*, 1977; Zhang *et al.*, 2017).

During the evaluation period from June 24 to September 3, 2019 (DAS 60-131), 119 mm of precipitation and 93 mm of irrigation were observed. Most of the precipitation fell in the early or late development stages, and the period of full plant development had a low quantity of rainfall (Fig. 5e). Due to the substantially insufficient rainfall in early summer, two irrigations had to be applied in the late plant stages, during seed development and maturation. Because the initial vegetative growth phase was not substantially limited by water stress, there was no change in the potential ranges of E/ET and T/ET for any of the following periods, which would have shifted the weight to E and impaired water productivity (Fereser and Soriano, 2006). However, with advancing water stress, actual ET (and thus photosynthesis) was affected, thereby resulting in reduced biomass production. The response of the plants to periods of water deficit was identifiable by comparing the yield parameters with data from a similarly managed but well-watered lysimeter. Although the numbers of husks and seeds were only slightly reduced compared with consistently well-watered conditions, the grain yield was lower (Table 3).

Table 3. Yield parameters from a field (minimal irrigation) and a nearby lysimeter (regular irrigation) with a similar soil profile as the adjacent field. Crop parameter assessment from 4 (field) or 2 (lysimeter) manually harvested 2 m² samples

| Yield parameter | Field | Lysimeter |
|-----------------------------------|-------|-----------|
| Number of plants | 86 | 87 |
| Total weight (g) | 930 | 1 002 |
| Husks/plant | 18.5 | 17.2 |
| Seeds/plant | 41.8 | 43.2 |
| Seeds/husk | 2.25 | 2.51 |
| TSW (g) | 135.2 | 157.5 |
| Rain yield (kg ha ⁻¹) | 2 411 | 2 961 |
| HI | 0.52 | 0.59 |

TSW – Thousand seed weight; HI – harvest index.

Optimal soybean development depends on sufficient water supply during the sensible phases of blossom (at approximately DAS 60) and grain filling (beginning at approximately DAS 80). Obviously, the irrigation events came too late for the seed maturation phase, as indicated by the losses of husk and seed yield. When compared with the reduction in total mass, losses in grain yield were more substantial. Losses due to irrigation which occurred too late were indicated by a decline in the harvest index due to dry matter partitioning (Table 3), which is generally caused by limited transpiration after anthesis (Fischer, 1979). Thus, one assumption that may be made is that an earlier intervention with irrigation would substantially reduce the yield loss. Furthermore, an earlier sowing date by two weeks would have decreased unproductive water loss from the bare soil, as shown by the results of the dual crop coefficient approach. During these two weeks, when the bare soil was exposed to radiation and turbulence, ET reached a value similar to that achieved during full vegetation.

The amount of precipitation or irrigation, and the initial water content, showed their effects on E/ET and T/ET. The lesser rain events, which only wetted the canopy and surface layer, mainly contributed to E/ET. More substantial rain and irrigation events, which percolated to the deeper-rooted soil layers, increased T/ET, as observed for the irrigation events and the following periods (Figs 5a, e, and g). In particular, precipitation and irrigation events on the pre-wetted topsoil led to higher T ratios. For example, an increase in T/ET was observed for the second irrigation event soon after a medium rain event. The applied water infiltrated more rapidly and deeper than it did in response to the first irrigation into the root zone (Fig. 5g), thus, it was available for root water uptake. As shown by Neukum *et al.* (2021) for different soils in a water-limited area, actual ET and soil moisture dynamics are limited by water availability, depending on the storage capacity and hydraulic conductivity of the soil. Evaporation is restricted by water availability in the surface soil layer, and transpiration is restricted by water availability in the root zone. Hence, irrigation should be applied such that water reaches the rooting zone without the frequent wetting of the soil surface. Under the given

local conditions, few intense irrigation events (during the night-time hours) are recommended. Considering the water storage capability within the root zone (approximately 230 mm), the number of individual irrigation events should be kept to a minimum for the total required amount of water. However, the restrictions of the irrigation technique (kinetic energy) with respect to the destabilization of soil structure at the topsoil level, percolation through preferential flow paths, water logging, or soil erosion in inclined areas, for instance, must be considered. Also, the strong dependence of irrigation timing and the extent of season-to-season variability on the precipitation regime and the long-term changes in the seasonal water balance (Eitzinger *et al.*, 2013) must also be taken into consideration. Furthermore, soil moisture dynamics during dry seasons with strongly limited evaporation (Neukum *et al.*, 2021) should be part of the management plan, except for plant-specific water-stress-sensitive periods, such as flowering until seed formation in soybean. These moisture dynamics in periods with strongly limited evaporation were observed during periods without rain or precipitation. After a wetting event, the surface soil desiccated (initial energy-limited constant-rate E phase) and caused high ET rates (Fig. 5c). This water loss may be reduced by fewer frequent events. For the following falling-rate phase of the soil evaporation process, E/ET and T/ET indicated (*e.g.*, for Periods VI and VIII, Fig. 5) the low ability of the local soil to deliver water from lower soil depths (evaporability), which further supports the strategy with few intense irrigation events.

CONCLUSIONS

1. In this study, evaporation/evapotranspiration and transpiration/evapotranspiration of a conventionally managed soybean field were determined using a water and stable isotope mass balance approach. The range of weekly transpiration/evapotranspiration from the blossoming period to the beginning of maturation was between 60% ($\pm 11\%$) and 82% ($\pm 10\%$). This range agrees with those of other studies on soybean, which have used other partitioning techniques and investigated partitions under well-watered conditions. However, evaporation/evapotranspiration and transpiration/evapotranspiration did not vary over time under the influence of canopy development only. Water availability caused considerable variations in evaporation/evapotranspiration and transpiration/evapotranspiration within this plant-specific range. During periods of water stress, water availability shifted evaporation/evapotranspiration and transpiration/evapotranspiration, depending on the vertical water distribution in the soil profile. The proportion of transpiration during periods with partial soil cover and substantial plant water availability surpassed the proportion of transpiration during times of complete soil surface cover and water stress. In times with a dry soil surface, evaporation decreased to almost zero, which verified the mass balance method. By

contrast, a saturated surface layer substantially increased evaporation/evapotranspiration even under a closed canopy. The multiple minor rain events during full canopy development were mainly lost by evaporation and accounted for the high evaporation/evapotranspiration during the summer. Moreover, this measured unproductive water loss did not include precipitation and irrigation water lost through interception.

2. For the local conditions, the evaluation led to the first conclusion that earlier sowing or mulch protection would have improved water use, because the initial vegetation phase was characterized by a high evaporative demand. Crop yield evaluation showed that earlier irrigation (as in the lysimeter) had a better effect on yield than the applied late irrigation in the field. Secondly, the local soil depth and water holding capacity proved adequate for storing the water of such intense irrigation events, which limits the number of events that wet the surface. And thirdly, the irrigation water applied on a pre-wetted surface increased the evapotranspiration efficiency. The initial soil water content before the second irrigation event was higher than before the first irrigation, thereby allowing the irrigation water to reach a greater depth within the entire root zone and thus it was more effectively used by the plants. In general, the experimental approach using the water and stable isotope method in combination with the monitoring of crop development, weather conditions, and water status was shown to be suitable for the assessment of management strategies. However, in order to obtain a quantitative relationship between irrigation and the amount of water used for transpiration, it is necessary to increase the focus on watering events and also shortening the sampling intervals is necessary. Short-term interactions between evaporation and transpiration, and variations in meteorological conditions or rapidly changing soil water conditions, inhibit the link between evaporation/evapotranspiration and transpiration/evapotranspiration for influencing factors and management activities.

Conflict of interest: The authors declare no conflict of interest.

REFERENCES

- Allen R.G., Pereira L.S., Raes D., and Smith M., 1998. Crop evapotranspiration - Guidelines for computing crop water requirements. (Irrigation and drainage, 56), Rome: FAO, ISBN: 92-5-104219-5.
- Allen R.G., Walter I.A., Elliott R.L., Howell T.A., Itenfisu D., Jensen M.E., and Snyder R.L., 2005. The ASCE standardized reference evapotranspiration equation. *Am. Soc. Civil Eng.*, <https://doi.org/10.1061/9780784408056>
- Allison G.B., 1998. Stable isotopes in soil and water studies, In: hydrologie et géochimie isotopique, hydrology and isotope geochemistry (Eds C. Causse, F. Gasse). Éditions de l'Orstom, Paris, 23-38.
- Ashley D.A., 1983. Soybean. In: crop-water relations (Eds I.D. Teare, M.M. Peet). Wiley, New York, 389-422.

- Bai H. and Purcell L.C., 2018.** Response of carbon isotope discrimination and oxygen isotope composition to mild drought in slow-and fast-wilting soybean genotypes. *J. Crop Improv.*, 32, 239-253, <https://doi.org/10.1080/15427528.2017.1407856>
- Bauer T. and Strauss P., 2014.** A rule-based image analysis approach for calculating residues and vegetation cover under field conditions. *Catena*, 113, 363-369, <https://doi.org/10.1016/j.catena.2013.08.022>
- Briggs L.J. and Shantz H.L., 1913.** The water requirement of plants. US Government Printing Office.
- Brisson N., Itier B., L'Hotel J.C., and Lorendeau J.Y., 1998.** Parameterisation of the Shuttleworth-Wallace model to estimate daily maximum transpiration for use in crop models. *Ecol. Modell.*, 107, 159-169, [https://doi.org/10.1016/S0304-3800\(97\)00215-9](https://doi.org/10.1016/S0304-3800(97)00215-9)
- Bunce J., 2019.** Consistent differences in field leaf water-use efficiency among soybean cultivars. *Plants*, 8, 123, <https://doi.org/10.3390/plants8050123>
- Clark I.D. and Fritz P., 2013.** Environmental isotopes in hydrogeology. Boca Raton, Florida. CRC press, <https://doi.org/10.1201/9781482242911>
- De Pascale S., Dalla Costa L., Vallone S., Barbieri G., and Maggio A., 2011.** Increasing water use efficiency in vegetable crop production: from plant to irrigation systems efficiency. *Horttechnology*, 21, 301-308, <https://doi.org/10.21273/HORTTECH.21.3.301>
- Dubbert M. and Werner C., 2019.** Water fluxes mediated by vegetation: emerging isotopic insights at the soil and atmosphere interfaces. *New Phytol.*, 221, 1754-1763, <https://doi.org/10.1111/nph.15547>
- Ehleringer J.R. and Dawson T.E., 1992.** Water uptake by plants: perspectives from stable isotope composition. *Plant. Cell Environ.*, 15, 1073-1082, <https://doi.org/10.1111/j.1365-3040.1992.tb01657.x>
- Eitzinger J., Trnka M., Semerádová D., Thaler S., Svobodová E., Hlavinka P., Šiška B., Takáč J., Malatinská L., Nováková M., Dubrovský M., and Žalud Z., 2013.** Regional climate change impacts on agricultural crop production in Central and Eastern Europe-hotspots, regional differences and common trends. *J. Agric. Sci.*, 151, 787-812. doi: <https://doi.org/10.1017/S0021859612000767>
- Ellsworth P.Z. and Williams D.G., 2007.** Hydrogen isotope fractionation during water uptake by woody xerophytes. *Plant Soil*, 291, 93-107, <https://doi.org/10.1007/s11104-006-9177-1>
- Evett S.R., Schwartz R.C., Casanova J.J., and Heng L.K., 2012.** Soil water sensing for water balance, ET and WUE. *Agric. Water Manag.*, 104, 1-9, <https://doi.org/10.1016/j.agwat.2011.12.002>
- Evett S.R., Schwartz R.C., Tolk J.A., and Howell T.A., 2009.** Soil profile water content determination: Spatiotemporal variability of electromagnetic and neutron probe sensors in access tubes. *Vadose Zo. J.*, 8, 926-941, <https://doi.org/10.2136/vzj2008.0146>
- Eyre S.R., 2017.** Vegetation and soils: a world picture. Routledge. Transaction Publishers, Rutgers University, New Jersey
- Fereres E. and Soriano M.A., 2006.** Deficit irrigation for reducing agricultural water use. *J. Exp. Bot.*, 58, 147-159, <https://doi.org/10.1093/jxb/erl165>
- Fischer R.A., 1979.** Growth and water limitation to dryland wheat yield in Australia: A physiological framework. *J. Aust. Inst. Agric. Sci.*, 45, 83-89.
- Foken T., 2008.** The energy balance closure problem: an overview. *Ecol. Appl.*, 18, 1351-1367, <https://doi.org/10.1890/06-0922.1>
- Foken T., Aubinet M., and Leuning R., 2012a.** The eddy covariance method. In: *Eddy covariance. Springer atmospheric sciences* (Eds M. Aubinet, T Vesala, D. Papale). Springer, Dordrecht, 1-19, https://doi.org/10.1007/978-94-007-2351-1_1
- Foken T., Leuning R., Oncley S., Mauder M., and Aubinet M., 2012b.** Corrections and data quality control. In: *Eddy covariance. Springer atmospheric sciences* (Eds M. Aubinet, T Vesala, D. Papale). Springer, Dordrecht, 85-131, https://doi.org/10.1007/978-94-007-2351-1_4
- Gonfiantini R., 1986.** Environmental isotopes in lake studies. *Handbook of environmental isotope geochemistry, The Terrestrial Environment, B*, 113-168, <https://doi.org/10.1016/B978-0-444-42225-5.50008-5>
- Gordon H.S., 1940.** Thermocouple psychrometers and evaporation studies. *Bull. Am. Meteorol. Soc.*, 21, 115-116.
- Gröning M., Lutz H.O., Roller-Lutz Z., Kralik M., Gourcy L., and Pölsenstein L., 2012.** A simple rain collector preventing water re-evaporation dedicated for $\delta^{18}\text{O}$ and $\delta^2\text{H}$ analysis of cumulative precipitation samples. *J. Hydrol.*, 448, 195-200, <https://doi.org/10.1016/j.jhydrol.2012.04.041>
- Hedley C.B., Knox J.W., Raine S.R., and Smith R., 2014.** Water: Advanced irrigation technologies, *Enc. Agric. Food Systems*, 378-406, <https://doi.org/10.1016/B978-0-444-52512-3.00087-5>
- Horita J. and Wesolowski D.J., 1994.** Liquid-vapor fractionation of oxygen and hydrogen isotopes of water from the freezing to the critical temperature. *Geochim. Cosmochim. Acta*, 58, 3425-3437, [https://doi.org/10.1016/0016-7037\(94\)90096-5](https://doi.org/10.1016/0016-7037(94)90096-5)
- IAEA, 2020.** WISER - Water Isotope System for data analysis visualization and Electronic Retrieval. <https://nucleus.iaea.org/wiser/index.aspx>
- Jiao X.-C., Song X.-M., Zhang D.-L., Du Q.-J., and Li J.-M., 2019.** Coordination between vapor pressure deficit and CO_2 on the regulation of photosynthesis and productivity in greenhouse tomato production. *Sci. Rep.*, 9, 1-10, <https://doi.org/10.1038/s41598-019-45232-w>
- Jovanovic Z. and Stikic R., 2018.** Partial root-zone drying technique: from water saving to the improvement of a fruit quality. *Front. Sustain. Food Syst.*, 1, 3, <https://doi.org/10.3389/fsufs.2017.00003>
- Kodešová R., Vlasakova M., Fer M., Tepla D., Jakšik O., Neuberger P., and Adamovský R., 2013.** Thermal properties of representative soils of the Czech Republic. *Soil Water Res.*, 8, 141-150, <https://doi.org/10.17221/33/2013-SWR>
- Kool D., Agam N., Lazarovitch N., Heitman J.L., Sauer T.J., and Ben-Gal A., 2014.** A review of approaches for evapotranspiration partitioning. *Agric. For. Meteorol.*, 184, 56-70, <https://doi.org/10.1016/j.agrformet.2013.09.003>
- Kucera C.L., 1954.** Some relationships of evaporation rate to vapor pressure deficit and low wind velocity. *Ecology*, 35, 71-75, <https://doi.org/10.2307/1931406>
- Lascano R.J., Van Bavel C.H.M., Hatfield J.L., and Upchurch D.R., 1987.** Energy and water balance of a sparse crop: simulated and measured soil and crop evaporation. *Soil Sci. Soc. Am. J.*, 51, 1113-1121, <https://doi.org/10.2136/sssaj1987.03615995005100050004x>
- Liebhart G., Klik A., Stumpp C., and Nolz R., 2022.** Partitioning evapotranspiration using water stable isotopes and information from lysimeter experiments. *Hydrol. Sci. J.*, 67(4), 646-661, <https://doi.org/10.1080/02626667.2022.2030866>

- Liu F., Andersen M.N., Jacobsen S.-E., and Jensen C.R., 2005.** Stomatal control and water use efficiency of soybean (*Glycine max* L. Merr.) during progressive soil drying. *Environ. Exp. Bot.*, 54, 33-40, <https://doi.org/10.1016/j.envexpbot.2004.05.002>
- Loiskandl W. and Nolz R., 2021.** Requirements for sustainable irrigated agriculture. *Agronomy*, 11, 306, <https://doi.org/10.3390/agronomy11020306>
- Loveys B.R., Stoll M., and Davies W.J., 2004.** Physiological approaches to enhance water use efficiency in agriculture: exploiting plant signalling in novel irrigation practice. In: *Water use efficiency in plant biology* (Ed. M. Bacon). Wiley-Blackwell, Oxford, 113-14.
- Majoube M., 1971.** Fractionnement en oxygene 18 et en deuterium entre l'eau et sa vapeur. *J. Chim. Phys.*, 68, 1423-1436, <https://doi.org/10.1051/jcp/1971681423>
- Masseroni D., Corbari C., and Mancini M., 2014.** Limitations and improvements of the energy balance closure with reference to experimental data measured over a maize field. *Atmosfera*, 27, 335-352, [https://doi.org/10.1016/S0187-6236\(14\)70033-5](https://doi.org/10.1016/S0187-6236(14)70033-5)
- Meier U., 2018.** Growth stages of mono- and dicotyledonous plants : BBCH Monograph, 2. Auflage. ed. Biologische Bundesanstalt für Land und Forstwirtschaft, <https://doi.org/10.5073/20180906-075119>
- Molden D., Murray-Rust H., Sakthivadivel R., and Makin I., 2003.** A water-productivity framework for understanding and action. In: *Water productivity in agriculture: limits and opportunities for improvement* (Eds J.W. Kijne R. Barker D. Molden). Wallingford, UK: CABI; Colombo, Sri Lanka: International Water Management Institute, 1-18. (Comprehensive Assessment of Water Management in Agriculture Ser. 1), <https://doi.org/10.1079/9780851996691.0001>
- Moore C.J., 1986.** Frequency response corrections for eddy correlation systems. *Boundary-Layer Meteorol.*, 37, 17-35, <https://doi.org/10.1007/BF00122754>
- Nangia V., 2020.** Water for food, water for life: The drylands challenge, <https://hdl.handle.net/20.500.11766/12017>
- Neukum C., Morales Santos A.G., Ronelngar M., and Vassolo S., 2021.** Modelling groundwater recharge, actual evaporation and transpiration in semi-arid sites of the Lake Chad Basin: The role of soil and vegetation on groundwater recharge. *Hydrol. Earth Syst. Sci. Discuss.*, 1-27, <https://doi.org/10.5194/hess-2021-581>
- Paltineanu I.C. and Starr J.L., 1997.** Real-time soil water dynamics using multisensor capacitance probes: Laboratory calibration. *Soil Sci. Soc. Am. J.*, 61, 1576-1585, <https://doi.org/10.2136/sssaj1997.03615995006100060006x>
- Pan X., Liu Y., Fan X., and Gan G., 2017.** Two energy balance closure approaches: applications and comparisons over an oasis-desert ecotone. *J. Arid Land*, 9, 51-64, <https://doi.org/10.1007/s40333-016-0063-2>
- Rawson H.M., Begg J.E., and Woodward R.G., 1977.** The effect of atmospheric humidity on photosynthesis, transpiration and water use efficiency of leaves of several plant species. *Planta*, 134, 5-10, <https://doi.org/10.1007/BF00390086>
- Ribas-Carbo M., Taylor N.L., Giles L., Busquets S., Finnegan P.M., Day D.A., Lambers H., Medrano H., Berry J.A., and Flexas J., 2005.** Effects of water stress on respiration in soybean leaves. *Plant Physiol.*, 139, 466-473, <https://doi.org/10.1104/pp.105.065565>
- Ritchie J.T. and Burnett E., 1971.** Dryland evaporative flux in a subhumid climate: II. Plant influences 1. *Agron. J.*, 63, 56-62, <https://doi.org/10.2134/agronj1971.00021962006300010019x>
- Rothfuss Y., Quade M., Brüggemann N., Graf A., Vereecken H., and Dubbert M., 2021.** Reviews and syntheses: Gaining insights into evapotranspiration partitioning with novel isotopic monitoring methods. *Biogeosciences*, 18, 3701-3732, <https://doi.org/10.5194/bg-18-3701-2021>
- Ruggiero A., Punzo P., Landi S., Costa A., Van Oosten M.J., and Grillo S., 2017.** Improving plant water use efficiency through molecular genetics. *Horticulturae*, 3, 31, <https://doi.org/10.3390/horticulturae3020031>
- Sakuratani T., 1987.** Studies on Evapotranspiration from Crops. *J. Agric. Meteorol.*, 42, 309-317, <https://doi.org/10.2480/agrmet.42.309>
- Sarkar D., Kar S.K., Chattopadhyay A., Rakshit A., Tripathi V.K., Dubey P.K., and Abhilash P.C., 2020.** Low input sustainable agriculture: A viable climate-smart option for boosting food production in a warming world. *Ecol. Indic.*, 115, 106412, <https://doi.org/10.1016/j.ecolind.2020.106412>
- Sauer T.J., Singer J.W., Prueger J.H., DeSutter T.M., and Hatfield J.L., 2007.** Radiation balance and evaporation partitioning in a narrow-row soybean canopy. *Agric. For. Meteorol.*, 145, 206-214, <https://doi.org/10.1016/j.agrformet.2007.04.015>
- Scanlon T.M. and Kustas W.P., 2010.** Partitioning carbon dioxide and water vapor fluxes using correlation analysis. *Agric. For. Meteorol.*, 150, 89-99, <https://doi.org/10.1016/j.agrformet.2009.09.005>
- Scanlon T.M. and Sahu P., 2008.** On the correlation structure of water vapor and carbon dioxide in the atmospheric surface layer: A basis for flux partitioning. *Water Resour. Res.*, 44, <https://doi.org/10.1029/2008WR006932>
- Schotanus P., Nieuwstadt F.T.M., and De Bruin H.A.R., 1983.** Temperature measurement with a sonic anemometer and its application to heat and moisture fluxes. *Boundary-Layer Meteorol.*, 26, 81-93, <https://doi.org/10.1007/BF00164332>
- Scott R.L., Knowles J.F., Nelson J.A., Gentine P., Li X., Barron-Gafford G., Bryant R., and Biederman J.A., 2020.** Water Availability impacts on evapotranspiration partitioning. *Agric. For. Meteorol.*, 108251, <https://doi.org/10.1016/j.agrformet.2020.108251>
- Sentek Pty Ltd, 2009.** Diviner 2000 user guide version 1.5. Stepney, South Australia. 5069, <https://sentektechnologies.com/download/diviner-2000-user-guide/>
- Seyfried M.S., Grant L.E., Du E., and Humes K., 2005.** Dielectric loss and calibration of the Hydra Probe soil water sensor. *Vadose Zo. J.*, 4, 1070-1079, <https://doi.org/10.2136/vzj2004.0148>
- Shuttleworth W.J. and Wallace J.S., 1985.** Evaporation from sparse crops-an energy combination theory. *Q. J. R. Meteorol. Soc.* 111, 839-855, <https://doi.org/10.1002/qj.49711146910>
- Šimůnek J., Šejna M., Van Genuchten M.T., Jacques D., Mallants D., Saito H., and Sakai M., 1998.** HYDRUS-1D. simulating one-dimensional movement of water, heat, and multiple solutes in variably-saturated media, Version 2.
- Šimůnek J., Van Genuchten M.T., and Šejna M., 2012.** The HYDRUS software package for simulating the two-and three-dimensional movement of water, heat, and multiple solutes in variably-saturated porous media. Technical Manual, Version 2, 258.

- Singer J.W., Heitman J.L., Hernandez-Ramirez G., Sauer T.J., Prueger J.H., and Hatfield J.L., 2010.** Contrasting methods for estimating evapotranspiration in soybean. *Agric. Water Manag.*, 98, 157-163, <https://doi.org/10.1016/j.agwat.2010.08.014>
- Stevens, 2015.** Comprehensive stevens hydra probe users manual, Rev. Portland, https://stevenswater.com/resources/documentation/hydraprobe/HydraProbe_Manual_Jan_2018.pdf
- Stroosnijder L., 1987.** Soil evaporation: Test of a practical approach under semi-arid conditions. *Netherlands J. Agric. Sci.*, 35, 417-426, <https://doi.org/10.18174/njas.v35i3.16736>
- Strudley M.W., Green T.R., and Ascough II J.C., 2008.** Tillage effects on soil hydraulic properties in space and time: State of the science. *Soil Tillage Res.*, 99, 4-48, <https://doi.org/10.1016/j.still.2008.01.007>
- Sutanto S.J., Wenninger J., Coenders-Gerrits A.M.J., and Uhlenbrook S., 2012.** Partitioning of evaporation into transpiration, soil evaporation and interception: a comparison between isotope measurements and a HYDRUS-1D model. *Hydrol. Earth Syst. Sci.* 16, 2605-2616, <https://doi.org/10.5194/hess-16-2605-2012>
- Tanner C.B. and Sinclair T.R., 1983.** Efficient water use in crop production: research or re-search?, In: limitations to efficient water use in crop production (Eds H.M. Taylor W.R. Jordan, and T.R. Sinclair). *Amer. Soc. Agronomy, Crop Sci. Soc. Amer., and Soil Sci. Soc. Amer.*, Madison, Wisconsin, 1-27, <https://doi.org/10.2134/1983.limitationstoefficientwateruse.c1>
- UNESCO, 2020.** The United Nations world water development report 2020: water and climate change, 978-92-3-100371-4
- von Hoyningen-Huene J., 1983.** Die interzeption des Niederschlages in landwirtschaftlichen Pflanzenbeständen., p 1-53. In: *Schriftenreihe deutscher Verband für Wasserwirtschaft und Kulturbau*, Num 57, Hamburg Berlin. 1983.
- Wassenaar L.I., Hendry M.J., Chostner V.L., and Lis G.P., 2008.** High resolution pore water $\delta^2\text{H}$ and $\delta^{18}\text{O}$ measurements by H_2O (liquid)- H_2O (vapor) equilibration laser spectroscopy. *Environ. Sci. Technol.*, 42, 9262-9267, <https://doi.org/10.1021/es802065s>
- Webb E.K., Pearman G.I., and Leuning R., 1980.** Correction of flux measurements for density effects due to heat and water vapour transfer. *Q. J. R. Meteorol. Soc.*, 106, 85-100, <https://doi.org/10.1002/qj.49710644707>
- Welp L.R., Lee X., Kim K., Griffis T.J., Billmark K.A., and Baker J.M., 2008.** $\delta^{18}\text{O}$ of water vapour, evapotranspiration and the sites of leaf water evaporation in a soybean canopy. *Plant, Cell Environ.*, 31, 1214-1228, <https://doi.org/10.1111/j.1365-3040.2008.01826.x>
- Wenninger J., Beza D.T., and Uhlenbrook S., 2010.** Experimental investigations of water fluxes within the soil-vegetation-atmosphere system: Stable isotope mass-balance approach to partition evaporation and transpiration. *Phys. Chem. Earth, Parts A/B/C*, 35, 565-570, <https://doi.org/10.1016/j.pce.2010.07.016>
- Wu Y., Du T., Ding R., Tong L., Li S., and Wang L., 2017.** Multiple methods to partition evapotranspiration in a maize field. *J. Hydrometeorol.*, 18, 139-149, <https://doi.org/10.1175/JHM-D-16-0138.1>
- Xiao W., Wei Z., and Wen X., 2018.** Evapotranspiration partitioning at the ecosystem scale using the stable isotope method - A review. *Agric. For. Meteorol.*, 263, 346-361, <https://doi.org/10.1016/j.agrformet.2018.09.005>
- Zhang D., Du Q., Zhang Z., Jiao X., Song X., and Li J., 2017.** Vapour pressure deficit control in relation to water transport and water productivity in greenhouse tomato production during summer. *Sci. Rep.*, 7, 43461, <https://doi.org/10.1038/srep43461>